Spatio-Temporal Patterns of Firearm Acquisition in the United States in Different Presidential Terms

Xu Wang,[1] Rifat Sipahi,[1] and Maurizio Porfiri[2]
[1)] *Department of Mechanical and Industrial Engineering, Northeastern University, Boston, MA, USA*
[2)] *Department of Mechanical and Aerospace Engineering and Department of Biomedical Engineering, New York University, Tandon School of Engineering, Brooklyn, New York, NY, USA*

(*Electronic mail: mporfiri@nyu.edu)

(*Electronic mail: r.sipahi@northeastern.edu)

(Dated: 23 May 2022)

This study develops mathematical tools and approaches to investigate spatio-temporal patterns of firearm acquisition in the U.S. complemented by hypothesis testing and statistical analysis. First, state-level and nation-level instant background checks (BC) data are employed as proxy of firearm acquisition corresponding to 1999-2021. The relative-phase time-series of BC in each U.S. state is recovered and utilized to calculate the time-series of the U.S. states' synchronization degree. We reveal that U.S. states present a high-level degree of synchronization, except in 2010-2011 and after 2018. Comparing these results with respect to a sitting U.S. President provides additional information: specifically, any two Presidential terms are characterized by statistically different synchronization degrees, except of G.W. Bush's first term and B.H. Obama's second term. Next, to detail variations of BC, short-time Fourier transform, dimensionality reduction techniques, and diffusion maps are implemented within a time-frequency representation. Firearm acquisition in the high frequency band exhibits a low-dimensional embedding, represented as a set of data points on the plane of two embedding coordinates. These data points, associated with different time windows of the BC data, form separate clusters signifying the state transitions in the original BC data. Through this analysis, we reveal that the frequency content of the BC data has a time-dependent characteristic. By comparing the diffusion map at hand with respect to a Presidential term, we find that at least one of the embedding coordinate presents statistically significant variations between any two Presidential terms, except of B.H. Obama's first term and D.J. Trump's pre-COVID term. The results point at a possible interplay between firearm acquisition in the U.S. and a Presidential term.

With a rate of firearm ownership of 1.21 firearms per capita, the U.S. has the largest firearm prevalence among all developed countries in the globe. There are more guns than people. Are gun purchases independently made throughout the country, or is there some form of coordination, collective behavior that drives firearm acquisition in U.S. states? Addressing this question is the first objective of this manuscript. Next, we investigate how patterns of firearm acquisition evolve over time. We bring forward methodological advances in statistics and engineering to answer the above two questions with data covering the last twenty years. Overall, this effort reveals compelling evidence that the U.S. states act in a highly coordinated manner when it comes to acquiring firearms and that such a coordination has time-dependent character. In view of these, we perform statistical analysis to compare this time-dependent coordination between the U.S. Presidents. Results suggest that there exists a possible interplay between a sitting U.S. President and temporal patterning of the BC data.

I. INTRODUCTION

According to a report from the U.S. Firearms Commerce, private citizens in the U.S. own a total number of 393 million firearms[1]. This figure corresponds to 1.21 firearms per capita, leading to a well-known fact in the U.S.: *we have more guns than people*. A decade ago, gun ownership in the U.S. was 0.9 per capita[2]: thus, gun ownership has risen over the last ten years even when adjusted against population growth. These numbers suggest a unique stand of the U.S. in terms of firearm prevalence, given that in other high-income countries, such as Germany, France, Canada, Italy, Australia, and Finland, ownership averages only around 0.27 per capita, even with large number of civilian firearm holdings[2].

The publicly available National Instant Criminal Background Checks (BC) data is a reliable resource that can help characterize firearm prevalence in the U.S. However, neither every background check results in a firearm acquisition, nor does each background check necessarily result in only a single firearm acquisition[3]. Despite these limitations, BC data has been extensively utilized by researchers as a proxy of firearm acquisition[4–11]. The data exhibit a clearly increasing trend, especially in the past decade, qualitatively supporting some of the survey results cited above. BC data has been utilized by Timsina *et al.*[4], for example, to study the relationship between firearm acquisition and youth gun carrying. Likewise, Porfiri *et al.*[5,11] examined the BC data to show how fear of stricter gun regulations after a mass shooting causes an increase in firearm purchases with nation- and state-level analyses. More recently, Schleimer *et al.*[6] and Lang and Lang[7] studied excess firearm purchases during the COVID-19 pandemic. Many authors also utilized BC data as a proxy to investigate firearm related homicides, suicides, and accidental

deaths[8–10].

BC data is available at the nation-level and state-level, each set of data enabling different research questions. The nation-level BC data is rich and informative, being available at a daily resolution, but it is only an aggregate of the state-level data. Studies based on monthly resolution state-level data can provide knowledge about how each state contributes to firearm acquisition in the U.S., and therefore help inform state-level policy making and characterize state-to-state interactions. Given that the U.S. states are diverse in many aspects including socio-economic factors, political views, and firearm laws, and that they may even react differently in different political climates, it is of strong interest to understand whether or not U.S. states behave similarly or differently in their firearm acquisition. Synchronization characteristics of U.S. states in their BC data can provide valuable insights into these similarities and differences.

Political climate can potentially influence the BC data. For example, nation-level BC data has experienced a dramatic increase immediately after B.H. Obama won the election in 2008. According to one source, this was possibly because gun-purchasing communities feared of stricter firearm regulations during President Obama's term[12]. Luca *et al.*[13] found the party in power at the state-level to be influential on the enactment of firearm-related laws upon occurrence of mass shootings. In addition, Eshbaugh-Soha and Peake [14] offered evidence about particular characteristics of three Presidents (R.W. Reagan, W.J. Clinton, and G.W. Bush) when setting agendas on unemployment, inflation, and international economics. Connecting these ideas together, a natural question that arises is how firearm acquisition patterns across states compare to Presidential terms. With BC data available since 1999, such an investigation can cover five terms of U.S. Presidency, namely two terms each of G.W. Bush and B.H. Obama and one term of D.J. Trump.

Here, we study synchronization patterns in BC data across states. Synchronization is calculated based on the phase between the states, where phase is defined as the instantaneous phase angle between two oscillators, both at the same frequency. Specifically, phase time-series of each U.S. state are extracted based on annual oscillations predominantly present in the data. These time series are next used to calculate synchronization time-series among the U.S. states based on the Kuramoto order parameter[15]. Moreover, analyzing the nation-level BC data at relatively high frequencies offers opportunities in understanding firearm acquisition characteristics among the U.S. states. Indeed, the fast varying content in the detrended and seasonally adjusted BC data was recently leveraged in an information theory based approach[5] to investigate causality between time-series of BC, media output, and mass shootings. Recognizing the rich information contained in the fast-varying content of BC data, we investigate the energy at relatively high frequencies in the spectrum of nation-level BC data using short-time Fourier transform. However, the arising power spectrum data is high dimensional and opaque to interpretation, thereby requiring a dimensionality reduction technique with clustering analysis to detect variations.

This study is focused on explaining whether or not U.S. states present a synchronized behavior in their firearm acquisition and how firearm acquisition compares with respect to the most recent five U.S. Presidential terms. To this end, literature on the main methods used in this paper is reviewed in Section II and data is described in Section III. Research methods and results pertaining to synchronization based on state-level BC data are provided in Section IV A and Section V A, with their robustness assessment included as Appendix. Time and frequency domain analysis of nation-level BC data based on short-time Fourier transform, dimensionality reduction, and clustering is presented in Section IV B and Sections V B. The manuscript ends with a discussion in Section VI.

II. LITERATURE REVIEW

A. Phase synchronization and Kuramoto order parameter

Interest in studying synchronization possibly started with the demonstration of how oscillations of two pendulums closely-positioned on a foundation eventually reach a "common rhythm" due to weak mechanical coupling between them via the foundation[16]. Study of synchronization is much broader than only mechanical systems. For example, synchronization appears frequently in economics[17], neuroscience[18–20] and human social behavior[21–23]. Based on the nature of data available, various mathematical tools, including phase synchronization[24], cross correlation[18], event synchronization[25], and nonlinear interdependence[26], are commonly utilized for investigating synchronization.

Given that the BC data for most U.S. states exhibit annual oscillations, a natural choice for our study is to analyze such oscillations in terms of their phase synchronization. Phase synchronization can be studied with oscillatory systems in a narrow frequency band[27]. This phenomenon is associated with the phase-locking degree and can be understood as the relative phase between these systems[21,28]. A well-established approach to measure the coherence of phase among a group of oscillatory units is to first recover their instantaneous phase and then utilize this phase information to calculate the Kuramoto order parameter[15,22,29,30]. The magnitude r of this order parameter will then help quantify the instantaneous degree of synchronization among the units in the group (see methods and analysis in Section IV).

The quantity r, which we call synchronization degree, varies between zero and one, where larger values indicate larger relative degree of synchronization. This mathematical tool has been utilized with promising results. For example, in an experiment where a number of participants sat together and rocked their chairs at the same time, the authors reveal distinctive synchronization degree for the movement of rocking chairs utilizing r in statistical tests[22]. In another study[31] based on multiple simulations, r is used to determine the effects of frequency mismatches on the synchronization of coupled oscillators.

B. Hilbert transform for phase recovery

Before phase synchronization among oscillating units can be studied, the phase of each of them needs to be calculated. This can be done by following two common techniques, namely, Hilbert transforms[32–34] or Wavelet transforms[19,35]. These two transforms are intrinsically related[27,36–38] and their premise is the definition of an analytical signal from the given time-series. This signal is a complex function whose amplitude and phase provide an estimate of the instantaneous amplitude and phase of the time-series.

Hilbert transform has proven to be a powerful tool in phase recovery in diverse research fields from neuroscience[38,39], signal processing[40], and acoustics[41] to aeronautics[34] and human behavior[21]. In terms of computational implementation, it can be calculated via several algorithms such as Fast Fourier Transform[32] and discrete convolution[42]. Hilbert transform is applicable to time-series with narrow frequency bands[43], but real-world data, such as the BC time-series at hand, are not necessarily narrow band. For this reason, a common practice is to first pre-process the time-series via filtering[27]. Other limitations in implementing Hilbert transform include the influence of product theorem of Hilbert transform[44,45] and edge effects[44]. In Section IV, we focus on Hilbert transforms and, to address these limitations, we include an equivalent analysis with Wavelet transforms in the Supplementary Information.

C. Diffusion maps for clustering

By applying mathematical and computational tools to analyze raw data, we often generate high-dimensional data that must be systematically interpreted to explain the underlying characteristics of the original, raw data. However, this is a challenging task due to the high-dimensional nature of the generated data. Originating from the notion of random walks, diffusion maps provide a useful and practical approach to analyze high-dimensional data in an effective manner via dimensionality reduction and spectral clustering[46]. Diffusion maps have been instrumental in helping explain high-dimensional data arising in the study of animal behavior[47,48], nonlinear dynamical system[49], network anomaly detection[50], and document classification[51].

Technically speaking, diffusion mapping extracts the intrinsic geometry in a given data set by constructing a network between the points in the data set and identifying pair-wise transition probabilities between any pairs of such points. This is achieved based on a so-called "diffusion distance," which, in some sense, combines all the paths of random walk transitions between the points. As per the definition of "diffusion distance"[46,52], diffusion maps offer a robust means to reveal the geometry underlying the data set even in the presence of noise and perturbations. In this sense, they are more preferred over other commonly utilized linear methods, such as principle component analysis[53], and nonlinear dimensionality reduction methods, such as ISOMAP[51,54]. Readers are referred to Kolpas *et al.*[47] and Aureli *et al.*[48], where authors demonstrate the efficacy of utilizing diffusion maps in studying collective motion.

Considering that real-world data such as the BC time-series at hand may be subject to noise and uncertainty, the choice of diffusion maps is well justified. Performing the diffusion map analysis of the BC time-series over large windows, on the order of years, will also help reduce the effects of noise. Research in collective group behavior provides further support and parallelism for the current study. For example, diffusion maps are utilized in[48] to reveal typical coherent patterns of animal groups and their transitions between these patterns. The current effort has analogous elements to the cited study in that we aim to reveal whether or not there exist certain patterns of behavior among the U.S. states in their BC data, and how these patterns, if they exist, compare with a Presidential term in the Office.

III. DATA

National instant criminal background checks (BC) data available publicly is utilized for analysis[55]. This data is available in two forms: (a) for each state at a monthly resolution and (b) aggregate of all the states as national data at a daily resolution. These data are plotted in the Appendix. The data ranges from $1/1999$ to $4/2021$, from 268 months in total. The state of Hawaii is not included in our study since BC data for this state is not available. Although the state of Connecticut has missing data from $1/2000$ to $8/2001$, this state is still included by considering zero values in place of the missing data.

When necessary, the data is treated in time windows corresponding to a Presidential term. Since the last year of D. J. Trump's term might be impacted by COVID-19, only the first three years of his Presidency are considered in our calculations. Data corresponding to D. J. Trump's fourth year in the Office are separately treated. G.W. Bush's first and second terms are respectively labeled with Bush (1) (1/2001-12/2004) and Bush (2) (1/2005-12/2008); B.H. Obama's first and second terms denoted by Obama (1) (1/2009-12/2012) and Obama (2) (1/2013-12/2016), and the first three years of D.J. Trump's term as Trump (pre-COVID-19) (1/2017-12/2019).

The datasets generated and/or analyzed in the current study are available on reasonable request.

IV. METHODS AND ANALYSIS

Two main directions are pursued: (1) using state-level monthly BC data, we calculate phase time-series of each U.S. state to estimate synchronization degree among the states (Section IV A); and (2) using nation-level daily BC data, we investigate how the energy in the BC data distributes over time and frequency, and implement diffusion maps and clustering techniques to explain how this power shifts over time in relation to a Presidential term (Section IV B). In the following, we provide the mathematical procedure to pursue (1)-(2).

A. Analysis of state-level monthly background check data

By observing BC time-series, a cyclic pattern is clear for most U.S. states where BC reaches peaks in winters and valleys in summers. That is, BC data exhibits a seasonality effect in *annual oscillations* with a frequency of $1/12 \approx 0.0833$ [1/months]; by factoring in some level of margin, we consider annual oscillations to be in the range of $[0.06, 0.11]$ [1/months]. With data sampled every month, the frequency spectrum of BC data is in the range of $[0, 0.5]$ 1/months. Hence, the frequency range of annual oscillations is about 10% of the whole spectrum. Next, BC time-series are detrended to ensure stationarity for power spectral density estimation. On average, the power of *annual oscillations* is found to be 35% of the total power for all U.S. states considered.

Since annual oscillations are the most prevalent for their relatively large power (35%) in a relatively small frequency band (10%), we focus on them for the study of synchronization. To this end, we view BC data of each U.S. state as an oscillator unit. Our approach is sketched in Fig. 1 and is made of three main steps (1)-(3):

(1) pre-process raw BC data by *reflection* and *filtering* (see Section IV A 1);

(2a) construct an analytical signal by implementing Hilbert transform on the pre-processed BC data of each U.S. state (see Section IV A 2);

(2b) compute phase time-series of each U.S. state (see Section IV A 2);

(3a) calculate the synchronization degree r time-series based on the definition of Kuramoto order parameter (see Section IV A 2); and

(3b) shuffle the phase samples from (2a) in multiple trials to generate surrogate data and repeat step (3a) on this data to obtain a distribution for r (see Section IV A 3).

At step (1), data is *pre-processed* by *reflection* and *pre-filtering*. Reflection is required to minimize artifacts in phase calculations in step (2)[44]. Pre-filtering to a desired narrow band[27,36] is necessary since Hilbert transform is applicable to only narrow-band signals[27]. At step (2), discrete-time Hilbert transform on the pre-processed BC data yields an analytical signal for each U.S. state (step (2a)), from which one can calculate the instantaneous phase time-series (step (2b)). Phase values are aggregated to compute the r time-series magnitude of the Kuramoto order parameter (step (3a)). The 95^{th} percentile of r distributions from step (3b) based on surrogate data can then be compared against r from step (3a), in each Presidential term, to exclude that synchronization of U.S. states is due to chance.

Once steps (1)-(3) are completed, we state the hypothesis that *the synchronization degree r depends on the Presidential term*. One-way ANOVA *F-test*[56] is conducted with all r values in their respective Presidential terms. The null hypothesis is that *the population means of r in the five terms are all equal*. A small p-value ($p < 0.05$) indicates that the null hypothesis can be rejected and hence different Presidential terms have impact on the value of r. If the null hypothesis is rejected, then a post-hoc test is conducted with Tukey's approach between pairs of terms, to reveal which two terms are different from each other ($p < 0.05$).

1. Pre-processing and pre-filtering of data

In the implementation of Hilbert transform, one must mitigate errors due to *edge effects* caused by the finite length of time-series to be analyzed. This issue can be addressed by following a procedure called *reflection*, or *symmetric extension*[44,57]. Let the original time-series of BC be denoted as $y[n]$ with $n = 1, ..., N_t$, and N_t being the total number of months included in the analysis. We process the time-series as follows:

$$\hat{y}[n] = \begin{cases} y[N_t - n + 1] & \text{if } 1 \le n \le N_t, \\ y[n - N_t] & \text{if } N_t + 1 \le n \le 2N_t, \\ y[3N_t - n + 1] & \text{if } 2N_t + 1 \le n \le 3N_t. \end{cases} \quad (1)$$

The output of this procedure, $\hat{y}[n]$, is a time-series where the original BC time-series $y[n]$ is placed in between its mirrored duplicates. In what follows, $\hat{y}[n]$ is utilized for further analysis.

Since Hilbert transform is effective on narrow band time-series, the data $\hat{y}[n]$ should further be pre-processed via a bandpass filter[27,36]. Practically speaking, it is difficult to interpret the meaning of the phase if $\hat{y}[n]$ contains frequencies that span annual or even slower long-term oscillations, as well as faster seasonal oscillations. To address this issue, one should focus on a particular frequency band. Given that annual oscillations are dominant in the BC data (see Section IV A), a bandpass filter is designed to extract these oscillations. Specifically, we implement a fixed-order finite impulse filter (FIR filter), chosen for its excellent linear phase response with respect to frequency. The filter band-pass corresponds to the frequency range $[0.06, 0.11]$ [1/months]. By filtering $\hat{y}[n]$, we obtain $\hat{y}_f[n]$, which is then used in Hilbert transform as explained in the following subsection.

2. Instantaneous phase and synchronization degree

Hilbert transform can help reveal the instantaneous phase of a given signal $\mathscr{S}[n]$. In principle, this transformation can be seen as a way to create an analytical signal $z[n]$ with complex entries, whose real part is $\mathscr{S}[n]$ and imaginary part is a signal that is 90 degrees phase shifted with respect to $\mathscr{S}[n]$. The phase of these complex entries determines the instantaneous phase of $\mathscr{S}[n]$. The key characteristics of $z[n]$ in the frequency domain are that it has twice the magnitude at positive frequencies compared to the original signal, and its entire negative frequency spectrum is filtered out.

A signal $z[n]$ with the above-listed spectrum characteristics can be obtained by applying a Fourier transform followed by an inverse Fourier transform[32], without having to manipulate the signal in time domain. For this, we introduce $Y[m]$ as the

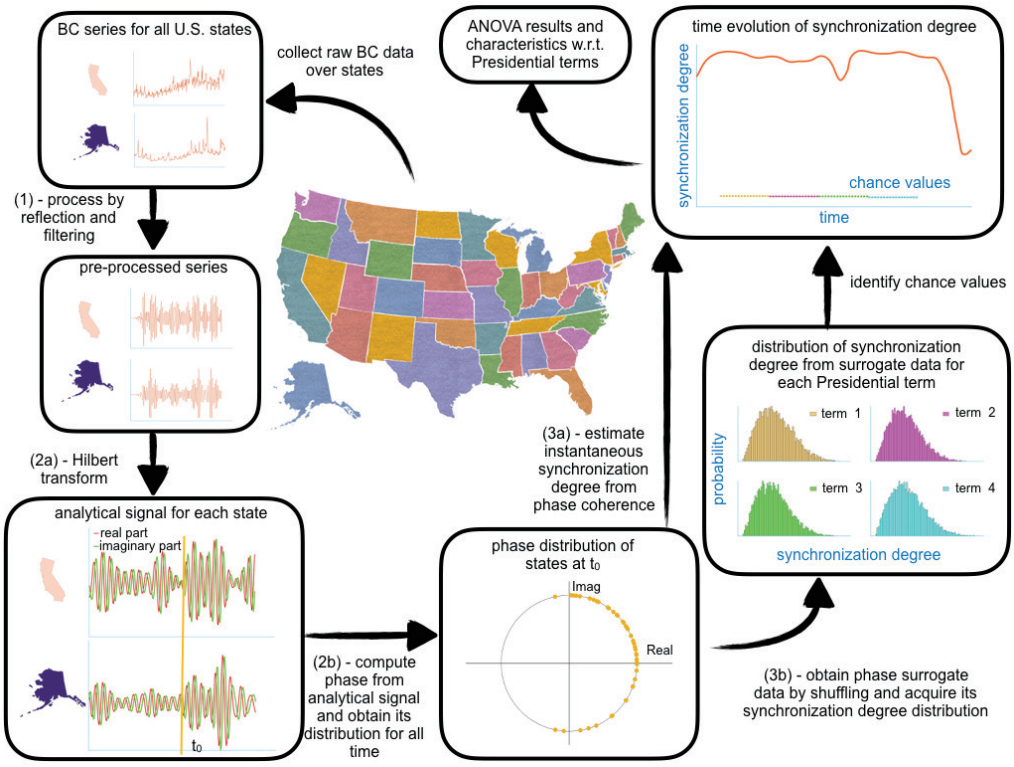

FIG. 1. The main procedure adopted to compute the synchronization degree among U.S. states and its assessment based on statistical analysis.

N_s-point Fast Fourier transform of $\hat{y}_f[n]$ with length N_s and construct the frequency domain signal $Z[m]$,

$$Z[m] = \begin{cases} Y[0] & \text{if } m = 0, \\ 2Y[m] & \text{if } 1 \le m \le \frac{N_s}{2} - 1, \\ Y[\frac{N_s}{2}] & \text{if } m = \frac{N_s}{2}, \\ 0 & \text{if } \frac{N_s}{2} + 1 \le m \le N_s - 1, \end{cases} \tag{2}$$

where N_s is even. The magnitude is set to zero for negative frequencies and doubled for positive frequencies. By applying next an N_s-point inverse discrete-time Fourier transform to $Z[m]$, we ultimately recover the analytical signal $z[n] = z_R[n] + i\, z_I[n]$, where i is the imaginary number. The phase of $z[n]$ is obtained by

$$\phi[n] = \arctan\left(\frac{z_I[n]}{z_R[n]}\right), \tag{3}$$

which is the instantaneous phase of $\hat{y}_f[n]$.

Working with the BC data set, we have a total of N phase time-series, $\phi_j[n]$, $j = 1, \ldots, N$, and N is the number of states. Then, the complex-form Kuramoto order parameter[15] is given by

$$k[n] = \frac{1}{N} \sum_{j=1}^{N} e^{i\,\phi_j[n]} = r[n] e^{i\,\psi[n]}, \tag{4}$$

where the instantaneous magnitude $r[n] = |k[n]|$ measures the *coherence of phases*, which we refer to as synchronization degree among the U.S. states. The parameter r takes values between 0 and 1, where $r = 1$ means units are perfectly synchronized with all their phases identical while $r = 0$ means no coherence among them with their phases uniformly distributed in their respective ranges (in the limit $N \to \infty$). The magnitude r of the Kuramoto order parameter is originally defined for large number of oscillators, $N \to \infty$[15,23]. However, r has also been utilized in experimental work with finite number of oscillators[22].

Finally, the last step is to remove the data that was inserted into the analysis to avoid edge effects (see Section IV A 1)[44] and adjust the time delay introduced by the FIR filter[33]. With this, the segment of $r[n]$ of interest is given by $r[n], n = N_t + \frac{o}{2} + 1, \ldots, 2N_t + \frac{o}{2}$, where o is the order of the FIR filter and the data at $n_0 = N_t + \frac{o}{2} + 1$ corresponds to January, 1999.

3. *Permutation test for the synchronization degree*

As a rule of thumb, the magnitude of the Kuramoto order parameter satisfying $r > 0.8$ is indicative of strong synchronization among coupled dynamical systems with large coupling strengths[58,59]. On the other hand, one should assess whether or not such r values can occur just by chance due to the specific structure of the data.

To generate chance values, one should create surrogate data through permutation of phase values of each U.S. state. Actual r values calculated in Section IV A 2 should then be contrasted against surrogate data to evaluate how

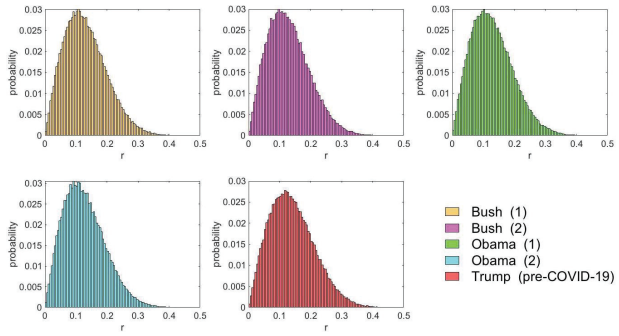

FIG. 2. Distribution of r based on surrogate data obtained via shuffling of phase time series, where legend labels and colors indicate which Presidential term they correspond to. The 95$^{\text{th}}$ percentiles of the distributions are respectively 0.254, 0.252, 0.251, 0.247, and 0.270 for Bush (1), Bush (2), Obama (1), Obama (2), and Trump (pre-COVID-19).

likely/unlikely these r values are to happen due to chance. Given a time window of a U.S. President, this window contains T number of phase values of 49 states. We can think that this data forms a 49 by T-dimensional matrix, $\Phi = \{\phi_j[n]\}$, where $\phi_j[n]$ is the phase of state j at time n, with $n = 1, ..., T$ and $j = 1, ..., 49$. Surrogate data is generated by following these steps:

(a) shuffle by randomly selecting one entry from each row of Φ to obtain 49 phase values, each from a different state, and collect these values in a vector J with 49 entries of phase values;

(b) use the phase entries in J to compute one r value; and

(c) repeat (a) and (b) in multiple trials to generate the distribution of r.

The above procedure is repeated separately for each time window of Presidency, yielding a distribution of r based on surrogate data (see Fig. 2). Next, we calculate the 95$^{\text{th}}$ percentile of each distribution, and state that values of r obtained in Section IV A 2 that are above this percentile in a particular time window are not to be attributed to chance.

B. Analysis of nation-level daily background check data

BC data carries rich information in the high frequency spectrum[5] and hence understanding how the power in this data distributes and potentially shifts over time with the Presidency is of strong interest. This question can be studied with BC data available at a daily resolution at the nation-level, where considered frequencies span seasonal and higher-frequency oscillations with periods in the range of $[20, 110]$ days (or, equivalently, frequencies in the range of $[0.27, 1.5]$ 1/month). First, the national BC data must be pre-filtered by removing the frequency components at relatively lower frequencies. This pre-filtering is performed based on fixed-order finite impulse response filter, following a procedure similar to the one in Section IV A 1.

Next, the short-time Fourier transform (STFT) of the filtered data is obtained. Specifically, a time segment with a fixed size of 730 days (i.e., two years) is moved over the data by 30 day increments, that is, adjacent time segments have an overlap of 700 days (see details in Section IV B 1). In each time segment, the Power Spectral Density (PSD) is calculated based on the Fourier transform. This calculation leads to a 3D visualization of the power with respect to frequency and time.

Due to the high-dimensional nature of the STFT data, a dimensionality reduction/clustering procedure is adopted. To this end, we utilize an approach based on diffusion mapping, where the intrinsic geometry in a given data set can be constructed as a network between the points in the data set and by identifying pair-wise transition probabilities between any pairs of such points. By combining all the paths of random walk transitions between the points, one can define what is known as the "diffusion distance," and express the geometry of the data in the diffusion space. This representation can be further reduced to a lower dimension by observing that only a few of the dimensions are sufficient to explain the main features of this geometry. Low dimensional embedding of the original data provides a practical means to view the structure of the data.

The procedure starting with national BC data and ending with the low dimensional embedding space is sketched in Fig. 3 and can be summarized in the following steps:

(1) nation-level daily BC data is filtered to the target frequency band;

(2) the filtered series is divided into multiple equal-length overlapping time segments (see Section IV B 1 for details);

(3) short-time Fourier transform is implemented separately on all time segments and the Fourier coefficients corresponding to each frequency are obtained. For a time segment i, these coefficients are squared to obtain the power at each frequency and collected in a vector $V(i)$. Next, each entry of $V(i)$ is normalized by the sum of its entries (see Section IV B 1 for details); and

(4) dimensionality reduction for $V(i)$ is performed by diffusion maps to find a low dimensional embedding and analyze the low dimensional character of the data set. More specifically, at this step, a similarity matrix is constructed based on the Euclidean distance between pairs of these vectors, $V(i)$ and $V(j)$. This similarity matrix is normalized to obtain the transition probability $M(i, j)$ from point i to point j, where M is the Markov matrix. The eigenvalues and eigenvectors of matrix M inform whether or not a low dimensional representation of the information in V is possible. If there is a spectral separation among the eigenvalues of M, then such a low dimensional representation is feasible where an embedding coordinate $Q(i)$ is obtained corresponding to $V(i)$ (see Section IV B 2 for details).

It is possible that the data points in the embedding coordinates associated with a Presidential term would form a coher-

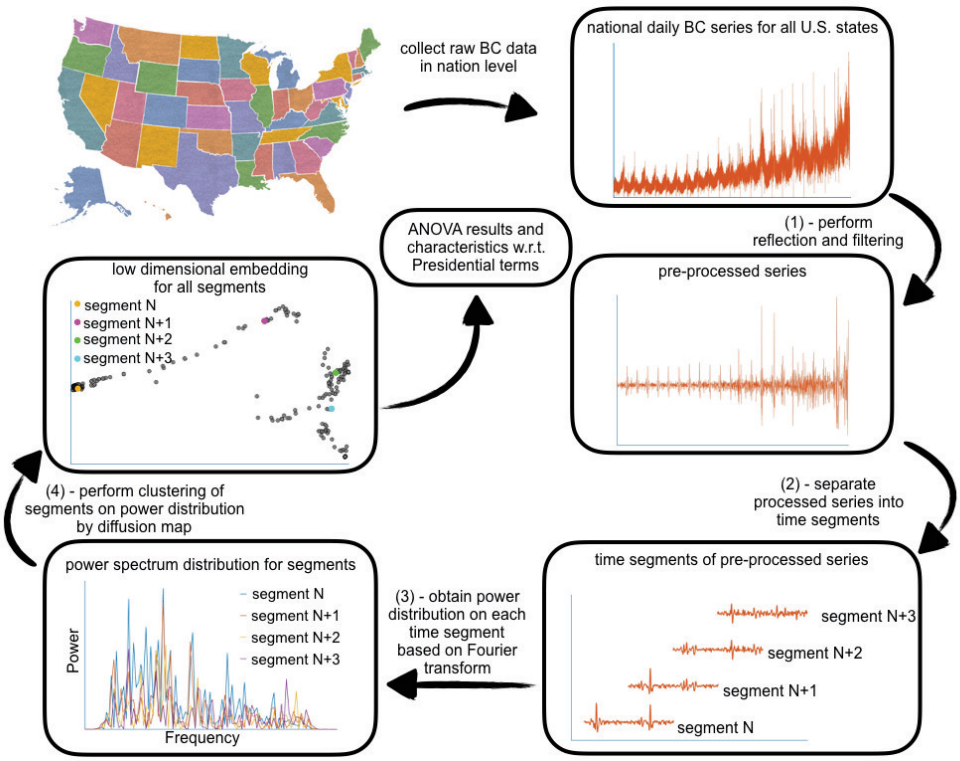

FIG. 3. The main procedure followed to perform the clustering analysis and its assessment based on statistical analysis.

ent cluster and separate from the clusters of data points corresponding to other terms. In each coordinate separately, a one-way ANOVA *F-test* is conducted with data grouped by their respective Presidential terms. The null hypothesis is that *the population means of data in an embedding coordinate in five Presidential terms are all equal*. A small p-value ($p < 0.05$) indicates that the null hypothesis can be rejected and hence different Presidential terms have impact on the samples in that coordinate. If the null hypothesis is rejected, then a post-hoc test is conducted with Tukey's approach between pairs of terms, to reveal which two terms are different from each other ($p < 0.05$). We remark here that the above dimensionality reduction and clustering analyses are conducted on the STFT data, not on BC time series. The reason for this choice is that relevant information lies in the frequency domain.

1. *Windowing and short-time Fourier transform*

Denote with $p_f[n]$ the pre-filtered data of the original time-series of daily national BC data $p[n], n = 1, ..., L$, where L is the total length in days. We use the FIR filter introduced in Section IV A 1, but since the focus is on higher frequencies, the pass band here is associated with oscillations of periods $[20, 110]$ days. Next, filtered national BC data is divided into time segments and Fourier transform in each segment is expressed by short-time Fourier transform (STFT),

$$STFT[p_f[n]](m,\omega) = P[m,\omega] = \sum_{n=-\infty}^{+\infty} p_f[n]w[n-m]e^{-j\omega n}, \tag{5}$$

where $STFT[\cdot]$ denotes the short-time Fourier transform, ω is the frequency, and $w[n]$ is the windowing function. A typical windowing function smooths the values of pre-filtered time-series to avoid spectral leakage in short-time Fourier transforms[60]. However, BC data potentially carries seasonal characteristics and hence the length of the time segment should be sufficiently large to capture such effects. In this study, the segment size is selected with a length of two years ($N_w = 730$ days).

BC data presents characteristically different frequency properties in winters versus summers. Therefore, when an edge-smoothing windowing function (such as Blackman Harris or Hamming window), is implemented on this data, the edges of the time segment corresponding to winters and summers will be smoothed as the time segment slides. Since winters and summers have different frequency properties, this implementation can lead to undesired loss of information. There are possibly two ways to fix this issue: one is to change the length of the time segment and the other is to use a different windowing technique. If the time segment is enlarged, it will register loss of time resolution, which is not preferred since we need sufficient time resolution to be able to resolve Presidential terms. If the length of the time segment is decreased, we will experience a loss of frequency resolution. Since BC

data presents seasonal effects, the time segment should not be selected smaller than one year.

A more convenient way to fix the above issue is to use a windowing technique that does not have an edge-smoothing feature. For this purpose, we utilize a rectangular window. However, this window is prone to spectral leakage, meaning that some portion of the power in the fundamental frequency of BC data will leak to the rest of the frequency spectrum. We calculate the leakage factor as 9.3%, indicating that only 9.3% of the total spectral power is spread over the side lobes of the spectrum. We suggest that this is a reasonable trade-off since it is more important to avoid artifacts due to edge-smoothing that can mask the seasonality effects in the data. Moreover, since the BC data here is pre-filtered before being convoluted with a rectangular window, we find that the power in the frequency spectrum of interest still dominates the power in the remainder of the spectrum. As a result, some level of spectral leakage does not significantly affect the analysis.

With the above understanding, the rectangular window is defined next,

$$w[n] = w_0\left(n - \frac{N_w}{2}\right), \tag{6}$$

$$w_0(x) = \begin{cases} 1 & \text{if } x \in [\frac{-N_w}{2}, \frac{N_w}{2}], \\ 0 & \text{if otherwise,} \end{cases} \tag{7}$$

where N_w is the length of each time segment. Here, the adjacent time segments are apart from each other by 30 days. That is, for all selection of $m \in [m_1, m_2, ..., m_T]$, $m_{i+1} - m_i = 30$, $m_1 = 365.5$, $T = 248$. Further, in a time segment i of the data, the power distribution of frequency components is collected in a high-dimensional vector $V(i)$ and each entry of $V(i)$ is normalized as follows: $V(i) = \frac{1}{\sum_\omega P^2(m_i,\omega)}[\, P^2[m_i,\omega_0], P^2[m_i,\omega_1], ..., P^2[m_i,\omega_{Nyquist}]\,]$.

2. *Spectral clustering with diffusion maps*

For the obtained set of vectors $V(i) \in \mathbb{R}^{N_b}, i = 1, ..., T$, where $N_b = 366$ is the number of discrete Fourier transform bins, we introduce the dimensionality reduction method, diffusion maps, to find the low-dimensional embedding of the data. This method is executed as explained next[46,52,61]. We define a similarity matrix $W \in \mathbb{R}^{T\times T}$,

$$W(i,j) = \exp(-d(V(i),V(j))/\sigma), \tag{8}$$

where $d(V(i),V(j))$ is the Euclidean distance between the vectors $V(i)$ and $V(j)$, with $\sigma = 0.2 d_{max}$ where d_{max} is the maximum Euclidean distance between two different vectors in the dataset $V(i)$. Clearly, $W(i,j) = W(j,i)$, that is, W is symmetric. By normalizing W by the diagonal matrix D, we obtain the Markov matrix $M = D^{-1}W$, where $D(i,i) = \sum_j W(i,j)$. Then, after transforming M into $M_s = D^{1/2}MD^{-1/2}$, we can write $M_s = D^{1/2}D^{-1}WD^{-1/2} = D^{-1/2}WD^{-1/2}$ and therefore it is easy to see that M_s is a symmetric matrix. Due to symmetry, this matrix has real eigenvalues and it can be decomposed as $M_s = S\Lambda S^\top$, where Λ is a block-diagonal matrix containing the eigenvalues λ_k of M_s, S is a matrix with orthogonal eigenvectors γ_i of M_s, and $^\top$ denotes matrix transposition.

Moreover, we can write $M = D^{-1/2}S\Lambda S^\top D^{1/2} = (D^{-1/2}S)\Lambda(D^{1/2}S^\top)^{-1}$. Thus, M_s has the same eigenvalues as M. Furthermore, the eigenvectors of M and M_s are related as $\phi_i = D^{-1/2}\gamma_i$. Noting that the largest eigenvalue of M is one by definition, the remaining eigenvalues are to be used to determine how to proceed with dimensionality reduction. Specifically, one sorts the eigenvalues in descending order as $\lambda_2, \ldots, \lambda_T$ and inspects the relative distance, i.e., the spectral gap between them. This will inform which of the larger eigenvalues are to be selected over smaller ones for dimensionality reduction, and the eigenvectors corresponding to the selected eigenvalues will define the low-dimensional embedding coordinates[46–48]. For $V(i)$, the coordinates of the corresponding points in the low dimensional space will be denoted by $Q(i) = (\phi_2(i), \phi_3(i), ..., \phi_k(i))$, considering $k-1$ eigenvectors are kept in the low-dimensional representation.

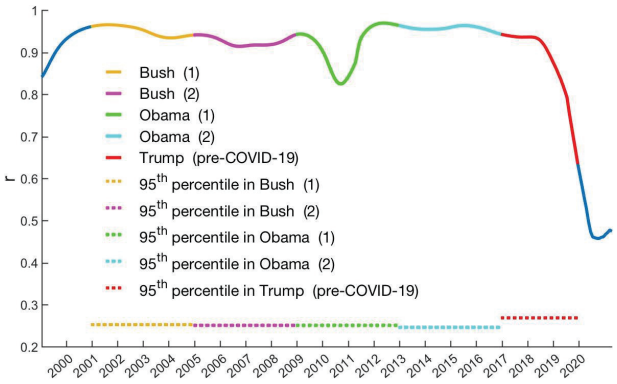

FIG. 4. Synchronization degree r over time, where the tick marks on the time axis mark the start of the years in January. These values are obtained based on the methods described in Section IV A 2. Horizontal lines correspond to 95$^{\text{th}}$ percentiles of the surrogate distributions in Fig. 2.

V. RESULTS

A. The synchronization degree varies with the Presidential term

The time-trace of the synchronization degree r of the U.S. states is shown in Fig. 4. We caution the reader that synchronization is associated with the relative phase between the U.S. states, but seasonality characteristics of the BC data does not automatically imply synchronization. During G.W. Bush's terms, the r value is always at relatively high levels with a mean of $r = 0.939$. One year after B.H. Obama takes the Office, however, the value of r starts dropping until 2011 when it reaches its lowest value of $r = 0.826$ in that term. Then,

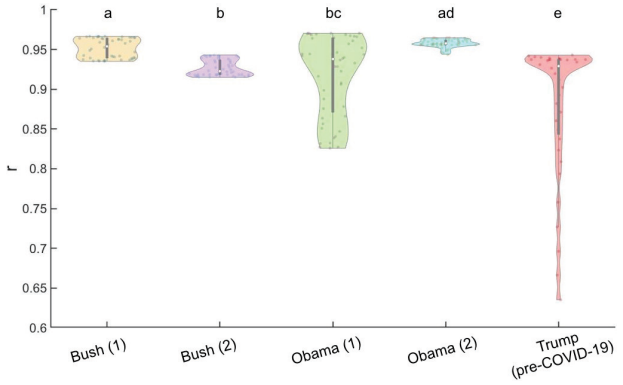

FIG. 5. Violin plots of r in Fig. 4 corresponding to the five terms of Presidency. One-way ANOVA *F-test* indicates that r values are affected by Presidential terms ($F(4,\ 223) = 22.93$, $p < 0.001$). Post-hoc comparisons reveal which pairs of terms are statistically different ($p < 0.05$; non-matching letters).

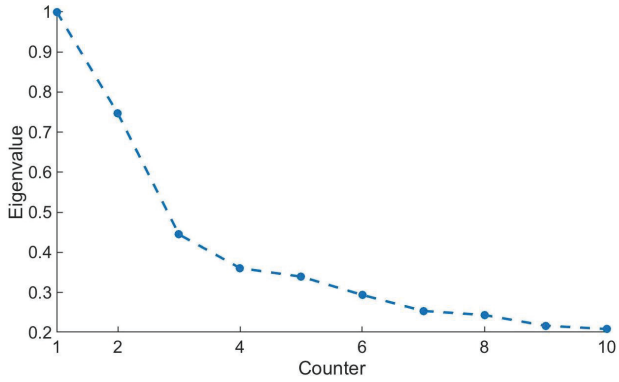

FIG. 6. The first 10 largest eigenvalues of the diffusion maps, where by default the largest eigenvalue $\lambda_1 = 1$ and the next two largest eigenvalues λ_2, λ_3 indicate a clear spectral separation from the remaining smaller eigenvalues.

it began growing back to values to around the same levels of G.W. Bush's terms. Throughout B.H. Obama's second term, the value of r holds steady at relatively high levels. Upon the arrival of D.J. Trump to the White House, the value of r holds steady initially, but within a year, it dropped to $r = 0.635$ in the pre-COVID-19 time period. The drop continues until D.J. Trump's last year in the Office during the COVID-19 pandemic. In permutation tests, all these values are different from chance values marked with horizontal dashed lines in Fig. 4. See also Supplemental Information where an alternative analysis provides support for the robustness of results in Fig. 4.

One-way ANOVA *F-test* is performed next to study how synchronization of U.S. states compares with Presidential terms. We find that r is affected by Presidential terms ($F(4,\ 223) = 22.93$, $p < 0.001$; see also the violin plots in Fig. 5). Furthermore, post-hoc comparisons identify that synchronization in the following pairs of Presidential terms is statistically different ($p < 0.05$): Bush (1)-Bush (2), Bush (1)-Obama (1), Bush (1)-Trump (pre-COVID-19), Bush (2)-Obama (2), Bush (2)-Trump (pre-COVID-19), Obama (1)-Obama (2), Obama (1)-Trump (pre-COVID-19) and Obama (2)-Trump (pre-COVID-19). That is, synchronization among the U.S. states in annual oscillations in their BC data is statistically different between any two terms of Presidency except when comparing Bush (2) with Obama (1), and Bush (1) with Obama (2).

B. Nation-level background checks data embed on a low-dimensional manifold that varies with the Presidential term

We present in Fig. 6 the eigenvalues of the diffusion map in descending order. A spectrum gap is obvious in this figure between the second eigenvalue $\lambda_2 = 0.75$ and the remaining smaller eigenvalues, and a smaller gap between the 3rd eigenvalue $\lambda_3 = 0.45$ and the remaining smaller eigenvalues. This result suggests that we can view the high-dimensional STFT data in a two-dimensional embedding space with respect to the second and third eigenvectors, ϕ_2 and ϕ_3, of the diffusion map. In Fig. 7, the embedding space is depicted where each data point in this space is representative of a time segment in which PSD was calculated. These points collectively describe a low-dimensional representation of the original high-dimensional STFT data. Recalling that the STFT data is made of multiple time segments, the STFT data points in the i^{th} time segment correspond to a single data point on the 2D embedding plane earmarked by $Q(i) = (\phi_2(i), \phi_3(i))$.

Analogous to the study of animal groups[47], the diffusion map here provides a representation of collective behavior of firearm acquisition in two independent coordinates $\phi_2(i)$ and $\phi_3(i)$ associated with λ_2 and λ_3, see Coifman and Lafon[46], where each coordinate provides critical information about the data. Specifically, in the first coordinate $\phi_2(i)$ we find that data is distinguished in two separate clusters; one corresponds to G.W. Bush's both terms ($\phi_2(i) < 0.5$) and the other covers B.H. Obama's two terms combined with that of D.J. Trump's ($\phi_2(i) > 0.5$). Furthermore, we observe that the data associated with Bush's second term is much more spread along this coordinate, suggesting that the evolution of firearm acquisition during this term exhibits different characteristics with respect to G.W. Bush's first term. With regard to coordinate in $\phi_3(i)$, we gather additional information for the point cloud at $\phi_2(i) > 0.5$. More specifically, $\phi_3(i)$ indicates that this point cloud is characterized by three separate clusters, where one is related to only B.H. Obama's second term ($\phi_3(i) < -1$), the other with B.H. Obama's first term combined with D.J. Trump's ($2 > \phi_3(i) > -1$), and the third one with black markers associated with the transition from G.W. Bush's second term to B.H. Obama's first term ($\phi_3(i) > 2$). With the help of diffusion maps, the diffusion coordinates help reveal relevant information as to the similarities and differences in the data associated with Presidents' terms (color coded).

Since each data point in Fig. 7 corresponds to a time segment i in which PSD is performed, we can color these data points depending on which U.S. Presidential term they belong to. In Fig. 7, a clustering feature is obvious based on color

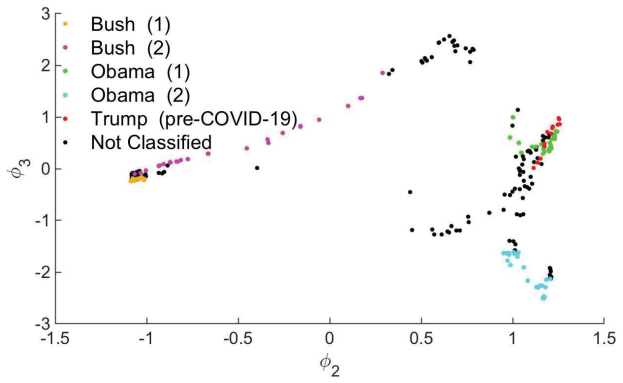

FIG. 7. Dimensionality reduction embedding results. The location of each point represents embedding coordinate of $V(i)$, corresponding to the i^{th} time segment of original data. Time segments associated with data prior to Bush (1), two consecutive Presidential terms, or the COVID-19 pandemic period are not classified (black markers).

coding of the markers. Clearly, Bush (2) separates out from the markers associated with Obama (1)-(2) and Trump (pre-COVID-19). Markers corresponding to Obama (2) are also separate from the data associated with Obama (1) and Trump (pre-COVID-19).

Lastly, following the methods presented in Section IV B, data is statistically analyzed along each embedding coordinate ϕ_2 and ϕ_3 separately. One-way ANOVA in each embedding coordinate points at variations with the Presidential term ($F(4,\ 108) = 596.24$, $p < 0.001$, for ϕ_2; $F(4,\ 108) = 278.57$, $p < 0.001$, for ϕ_3). Post-hoc tests reveal that any two Presidential terms are statistically different ($p < 0.05$) in at least one of the embedding coordinates, except between Obama (1) and Trump (pre-COVID-19), see also Fig. 8.

VI. DISCUSSION

With its unique legal landscape forged by historical elements, the U.S. is a country where private citizens satisfying certain conditions are eligible to purchase firearms. Since data as to how many firearm sales transactions are made in the U.S. is not publicly available, researchers have turned toward tracking background checks data, available from the Federal Bureau of Investigation (FBI), as a proxy of firearm acquisition in the U.S[10]. This data only captures the number of background checks performed: a background check may not necessarily indicate a firearm purchase and a single background check can lead to multiple firearm purchases[3]. Despite these limitations, BC data is still considered to be a reliable resource with which researchers can perform various analyses associated with firearm prevalence in the U.S[4–11].

There are various reasons that studying firearm prevalence in the U.S. is of value to the research community. For example, it is of strong interest to understand why affinity to firearms is much stronger in the U.S. than it is in other comparable benchmark countries[2]. This question relates to how humans choose to acquire firearms or not, and how potentially their socio-economical status, country's history and legal landscape, educational level, income level, and political views contribute to such choices[62]. Moreover, humans react only to certain events, and they react differently toward different events. How such reactions contribute to their choices can guide us to better understand human behavior and elucidate how such decisions contribute to governance, legal landscape, political debate, and ultimately influence firearm acquisition in the U.S.

In this manuscript, we studied spatio-temporal patterns of BC data in the U.S. and compared the results with Presidential terms. This was done by taking a rigorous mathematical/computational approach on the available BC data. Although the U.S. states have their unique characters, some are similar to some others in many ways, such as geographically, politically, and socio-economically. We investigated whether or not there exists coordination among the states in terms of their BC data. With annual oscillations predominantly present in the data, the focus was to understand how such oscillations compare in terms of their relative phases with respect to each other. To study these phase relationships, we calculated a metric called synchronization degree, with strong roots in the study of synchronization in diverse fields of nonlinear dynamical systems[15]. We determined that the U.S. states are highly synchronized in their BC data, except for about two years during the first term of B.H. Obama and during almost all the pre-COVID term of D.J. Trump. Alternative approaches were also provided to show evidence that the results have a strong degree of robustness. Statistical tests indicate that synchronization levels among the U.S. states vary with Presidential terms, except when comparing the second term of G.W. Bush with the first term of B.H. Obama and the first term of G.W. Bush with the second term of B.H. Obama.

Although we have not looked into the root causes of synchronization, it is reasonable to assume that nation-level common drivers contribute to orchestrated behaviors of firearm-purchasing communities. In view of Rogers [63] and Melgar [64], for example, it is tenable that firearm sales follow seasonality cycles with peaks during the holiday season. The presence of such peaks in the BC data[55] aligning with the holiday season further support seasonality effects (see Appendix for state-level BC data). On the other hand, root causes of synchronization cannot be attributed to only common drivers. More specifically, published work indicates key coupling among some U.S. states, for example, in terms of business cycles[65], house prices[66], as well as firearm acquisition[11]. Hence, it is plausible that synchronization among the U.S. states in terms of BC data is a combination of the effects of common drivers as well as state-to-state couplings.

It is critical to note that seasonality in the data does not imply synchronization. Synchronization is associated with the phase difference between time series of the same frequency; in this vein, temporary loss of synchronization is indicative of increased variability in the phase of oscillations. Such a disarray in the BC data is detected around 2010-2011 after one and half years into the first term of B.H. Obama, and in a much more pronounced manner during the pre-COVID term of D.J. Trump. While synchronization sheds light on the

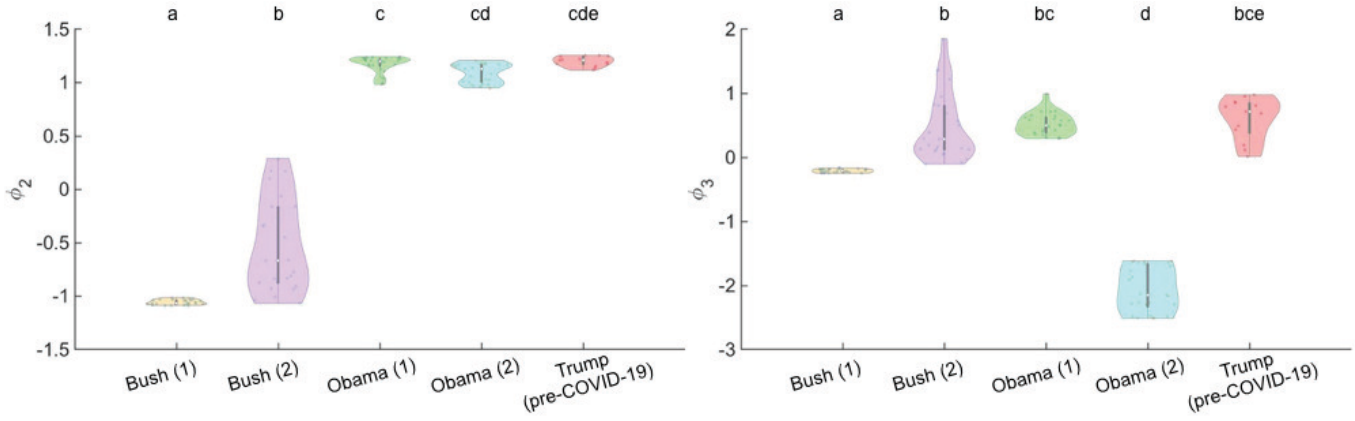

FIG. 8. Violin plots of data in the embedding coordinates ϕ_2 (left panel) and ϕ_3 (right panel) corresponding to the five terms of Presidency. One-way ANOVA *F-test* indicates that these data are affected by Presidential terms ($F(4,\ 108) = 596.24$, $p < 0.001$ for ϕ_2; $F(4,\ 108) = 278.57$, $p < 0.001$ for ϕ_3). Post-hoc comparisons reveal which pairs of terms are statistically different in the embedding coordinates ($p < 0.05$; non-matching letters).

degree of organization/disorganization among the U.S. states in their BC data, such an analysis has further implications; in particular, in our pursuit to thoroughly understand variations in firearm acquisition in the U.S. For example, it would be possible to investigate the relationship of synchronization, or lack thereof, to various attributes and/or extrinsic effects. In the current study, we have compared synchronization with Presidents' terms, and opportunities in this direction include the study of which U.S. states might be potentially influencing each other (network characterization, network identification), which states might be behaving more independently in their firearm acquisition (leaders versus followers), and how legal landscape influences the behavior of those states (stricter vs. permissive laws).

BC data contains rich information, especially at relatively high frequencies. This was leveraged, for example, in a recent study where information carried by high frequency noise has been statistically studied to explain the causal links between background checks, media output, and mass shootings[5]. Motivated by this observation, we examined nation-level BC data at relatively high frequencies with the goal of understanding how the energy in the frequency spectrum possibly shifts over time and how such an energy-shift compares with a Presidential term. Short-time Fourier transform was combined with diffusion mapping and clustering techniques to compactly represent the dominant geometric features of the BC data, on two-dimensional diffusion coordinates. This representation in essence demonstrates how the energy in the BC data diffuses over time. Specifically, in diffusion coordinates we observe data clusters from one term to another term of a President. Statistical tests indicate that such clusters are different between any pairs of Presidential terms in at least one of the diffusion coordinates, except between the first term of B.H. Obama and the pre-COVID term of D.J. Trump.

The nation-level analysis indicates the differences and similarities of firearm sales in the U.S. vis-à-vis a sitting President's term. One possible explanation for this is a President's ability to directly interact with masses and to potentially steer the trajectory of gun laws either toward stricter or permissive regulations. One piece of evidence to these arguments is in line with Depetris-Chauvin [12], where it is argued that the election of B.H. Obama created a perception that stricter firearm laws will be implemented.

We identify two main limitations of our research. First, since the actual figures of firearm purchases are not publicly available, we have relied on BC data as proxy of firearm acquisition in the U.S., following the practices of previous publications. Second, as mentioned in the study of nation-level BC data, we chose to accept some level of error in our analysis due to spectral leakage in the implementation of short-time Fourier transform operations. By assessing that leakage was less than 10%, we decided that this was an acceptable level of error as it helped to avoid the influence of seasonal differences in firearm purchases on clustering.

Although this study focuses on firearm prevalence, it can potentially translate to elucidate the relationship between firearm acquisition and gun-related harms. To better understand the complex mechanisms that lead to a harm, researchers in public health, criminology, policy making, and engineering have been studying the nature of shootings[67–69], impacts of firearm-related harm on healthcare[70], psychological drivers of violence[71,72], effectiveness of law and regulations on firearm[73], moderating role of media on violence[74], and root causes of firearm acquisition[5,75]. In criminology, specifically, studies include the investigation of how gun carrying and drug dealing are related[76,77], spatio-temporal spreading characteristics of gun violence[78], analysis on spatial clustering effects of gun violence within urban environments[79], and how certain urban physical features of properties could attract gun crimes[80].

We suggest several research directions in future work. Although we have not performed a causality analysis, future studies should look into whether or not there exists any causal link from a President's political agenda to firearm prevalence, and vice versa. Moreover, the analysis of the BC data can be expanded into frequency bands other than those studied

in this effort. While we have not studied in what ways each Presidential term could have influenced U.S. states' synchronization in their BC data nor have we looked into similarities/differences between a Democratic and Republican President, future work can analyze the Presidents' agendas, public statements, and support for stricter/permissive gun laws, to unveil the root causes of loss of synchronization. Referring to possible similarities/differences in firearm-purchasing communities, another direction of research could focus on characterizing those communities in their firearm acquisition as various relevant national and local events unfold.

In conclusion, we put forth a mathematical/computational approach to study BC data at the nation- and state-level, and revealed the synchronization characteristics of U.S. states and how energy contained in the BC data shifts over time. These results are backed by statistical tests and robustness analysis, all supporting the existence of time-dependent coordination among the U.S. states. The results further point out that this time dependence compares with Presidential terms, that is, there exists a possible interplay between a President's term and the complex dynamics associated with firearm acquisition in the U.S.

ACKNOWLEDGMENTS

This study has been supported in part by the U.S. National Science Foundation under award CMMI-1953135.

AUTHOR DECLARATIONS

Conflict of Interest

The authors have no conflicts to disclose.

DATA AVAILABILITY STATEMENT

The data that support the findings of this study are openly available in Federal Bureau of Investigation website at https://www.fbi.gov/services/cjis/nics.

Appendix: Robustness analysis

The phase calculated based on the principles of Hilbert transform can be influenced by how rapidly the amplitudes of the time signal are changing[44,45] and hence this issue should be addressed. Moreover, an alternative approach would help provide a degree of robustness on the reliability of the results. To this end, Wavelet transform can be leveraged to estimate the degree of synchronization r.

1. Influence of variant amplitudes

To investigate whether or not amplitude changes cause substantial variations in phase calculations, one can calculate r by normalizing the amplitudes of the BC data after pre-filtering and reflection procedures and before applying the Hilbert transform. That is, one should normalize first all the oscillation amplitudes in the filtered signal $\hat{y}_f[n]$, such that amplitudes do not change over time. This is an adjustment that only scales the amplitudes and hence should not influence the phase calculations. The amplitude-tuned signal then reads,

$$\hat{y}_t[n] = \frac{M_{\hat{y}_f}}{F_i}\,\hat{y}_f[n], \quad \text{for } n \in [n_i, n_{i+1}], \tag{A.1}$$

where n_i is the i^{th} zero point of $\hat{y}_f[n]$, F_i is the maximum absolute value of $\hat{y}_f[n]$ in the range of $[n_i, n_{i+1}]$, and $M_{\hat{y}_f}$ is the maximum absolute value of $\hat{y}_f[n]$. The signal $\hat{y}_t[n]$, which is adjusted for uniform amplitude, is utilized to compute the phase based on Hilbert transform. This phase is then used to calculate the synchronization degree r (blue in Fig. 9). In this figure, we compare r with that in Fig. 4 (red). Given that the two curves of r are almost identical to each other, we conclude that r calculation is only negligibly affected when amplitudes are normalized, providing support for the consistency of results.

2. Synchronization degree based on Wavelet transform

An alternative Morse wavelet transform can be implemented on the frequency domain representation of time-series data, to obtain $\phi_{W_s}(t)$, the corresponding phase series. The procedure is as follows. Based on Lilly and Olhede[35], for a square-integrable signal $x(t)$, the wavelet transform is defined as

$$\begin{aligned} W_s(t) &= \int_{-\infty}^{+\infty} \frac{1}{s}\psi^*\left(\frac{u-t}{s}\right) x(u)\,du \\ &= \frac{1}{2\pi}\int_{-\infty}^{+\infty} \frac{1}{s}\Psi^*(s\omega)X(\omega)\,d\omega, \end{aligned} \tag{A.2}$$

where s is the normalization constant, $\psi(t)$ is the selected wavelet function in time domain, $\Psi(\omega)$ is the Fourier transforms of $\psi(t)$, $X(\omega)$ is the Fourier transform of $x(t)$, and $(\cdot)^*$ denotes the complex conjugate of $(\cdot)$.

In this manuscript, we implement the wavelet in the frequency domain ω and the type of wavelet function selected is the Morse wavelet given by

$$\Psi_{P,\gamma}(\omega) = 2U(\omega)\left(\frac{e\gamma^2}{P^2}\right)^{\frac{P^2}{\gamma^2}} \omega^{\frac{P^2}{\gamma}} e^{-\omega^\gamma}, \tag{A.3}$$

where $U(\omega)$ is the unit-step function, P^2 is the time-bandwidth product, and γ represents the symmetry of this wavelet. With this setting, complex number $W_s(t)$ can be calculated as

$$W_s(t) = A_W(t)e^{i\phi_{W_s}(t)}, \tag{A.4}$$

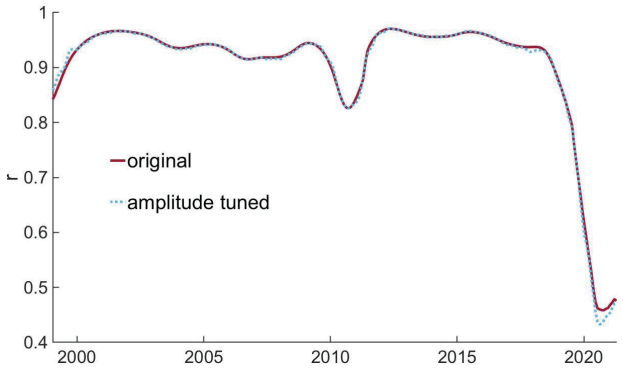

FIG. 9. Magnitude of Kuramoto order parameter r as a function of time obtained either based on the signal $\hat{y}_f[n]$ (blue) or $\hat{y}_t[n]$ (red). Here the blue curve is obtained based on amplitude adjustment and the red curve is carried from Fig. 4 for comparison.

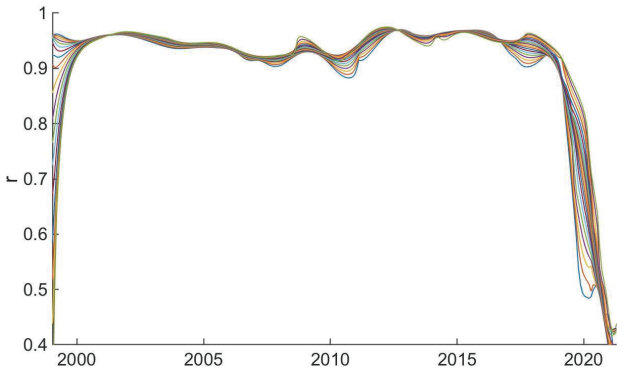

FIG. 10. Variability of the synchronization degree over time for a selection of central frequencies used to design Morse wavelet transform.

from which the phase $\phi_{W_s}(t)$ can be extracted.

Specifically, utilizing discrete version of wavelet transform in Matlab on state-level BC time-series, phase time-series for each U.S. state are obtained. These phase time-series are then utilized to compute $r[n]$. Since we utilize the reflected BC data in this procedure, the parts of $r[n]$ associated with the reflected data are neglected. Here, wavelet parameters are selected as $\gamma = 3$ for maximum degree of symmetry of shape of the Morse wavelet[35] and $P^2 = 30$, which are appropriate values to balance the two needs for narrow frequency pass-band width and short decay time. Next, the central frequency of the wavelet is adjusted with different selections of the normalization parameter s.

Since our focus is on BC data associated with annual oscillations, the central frequency is selected for an oscillation period in the range of $[10.6, 13.7]$ months, which is slightly narrower than that used in the FIR filter in Section IV A 1. To study the variability in the results, we sample this range into 18 linearly spaced data points, each describing a Morse wavelet with a different central frequency. For each of the wavelets, phase calculations are performed and a synchronization degree $r[n]$ is obtained. The family of 18 different curves are obtained as depicted in Fig. 10.

Fig. 10 provides support for the degree of robustness of results in Fig. 4. It also reveals that at two critical time points, the results have more sensitivity, or, equivalently there is more variation in the family of curves in Fig. 10. These time points arise around the valley in the winter of 2010 and after the spring of 2018. Nevertheless, the trend lines still clearly indicate the presence of the valley around 2010 in Obama (1) and a substantial drop in r in Trump (pre-COVID-19).

Appendix: State-level background checks

The plots of background check series by state (state of Hawaii is excluded) are provided here for direct observation and capture of the synchronization in Figs. 11, 12 and 13.

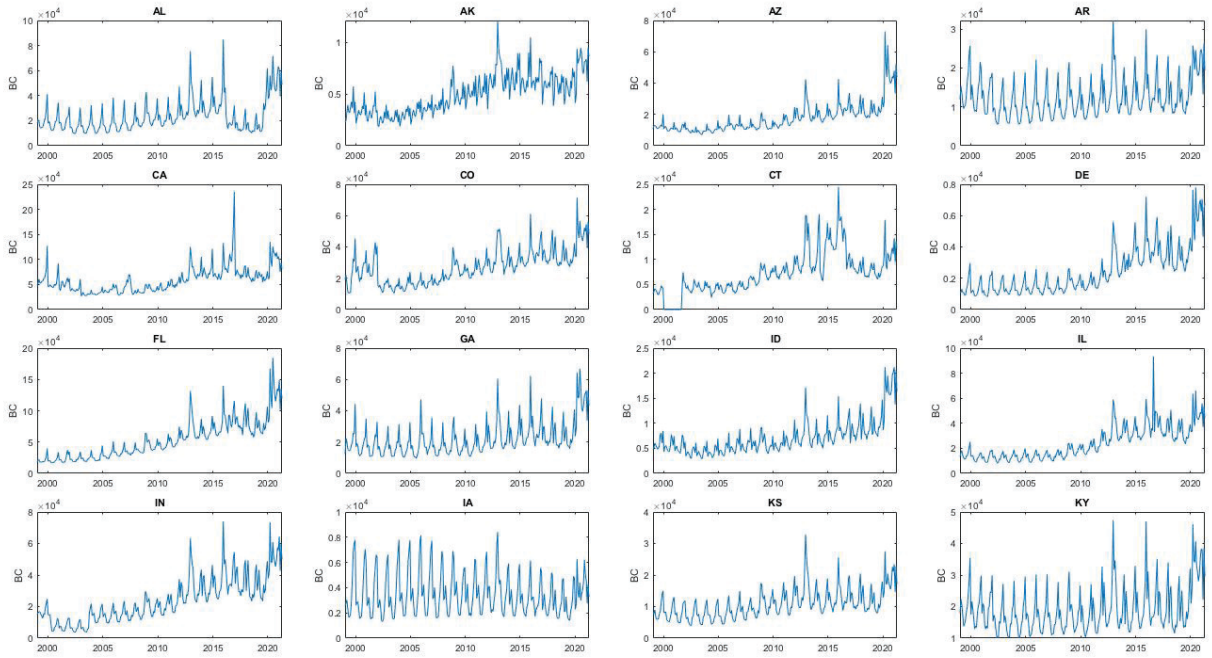

FIG. 11. Time series of background checks by state, from Alabama to Kentucky.

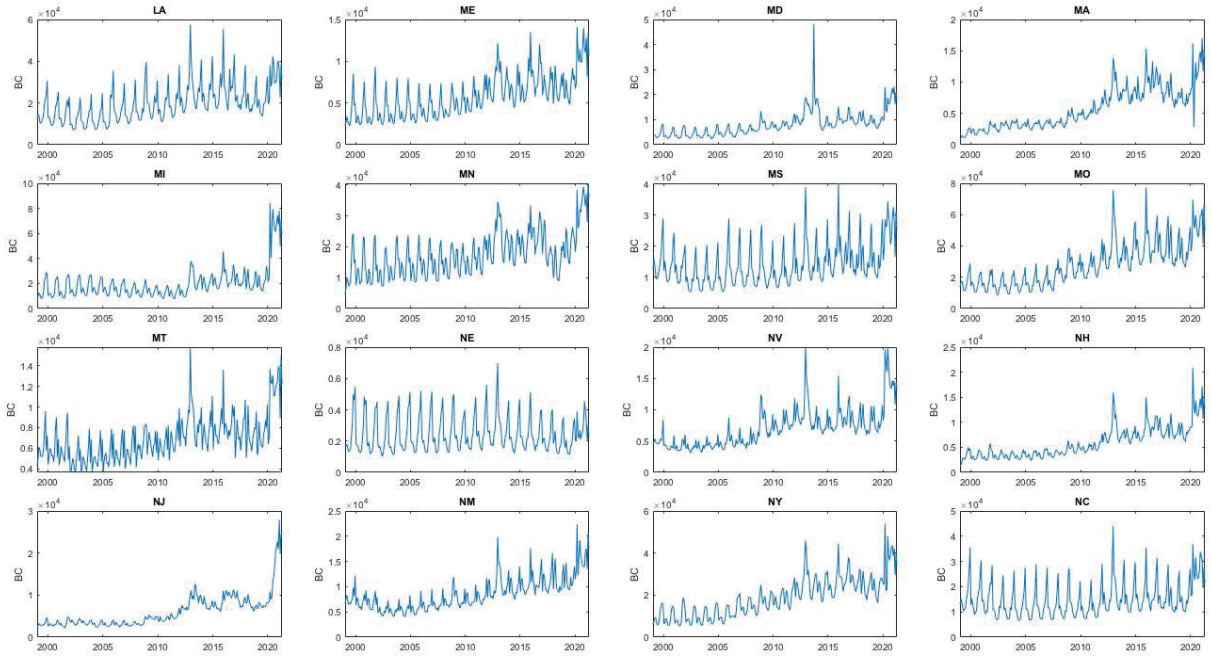

FIG. 12. Time series of background checks by state, from Louisiana to North Carolina.

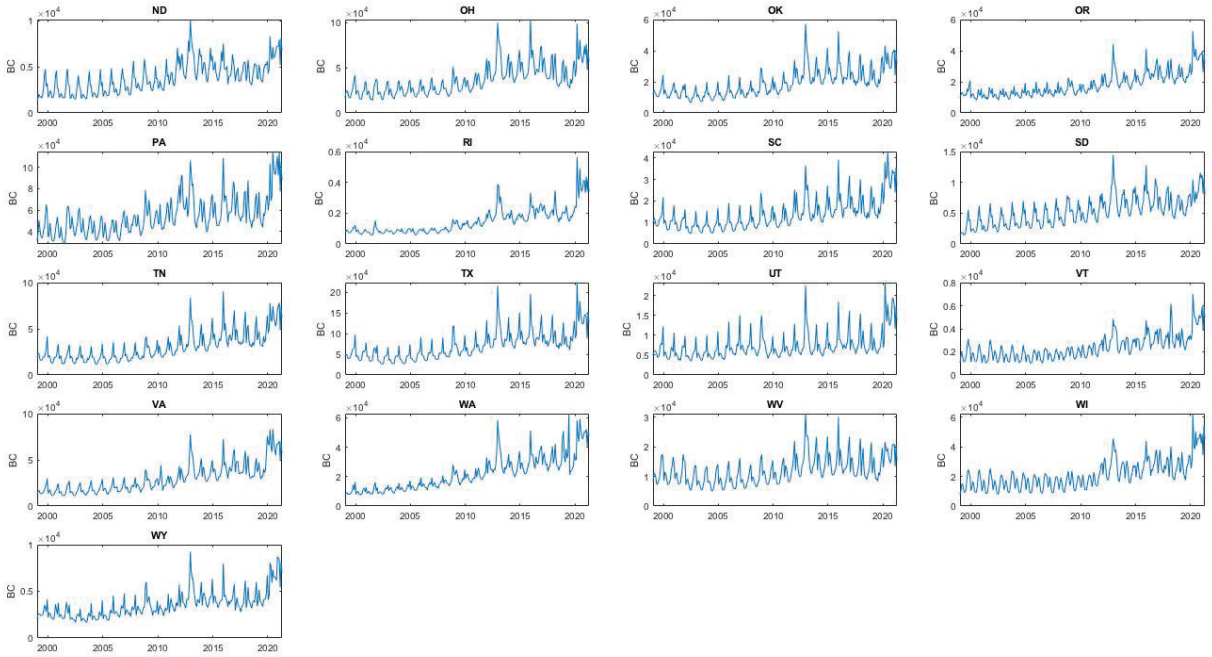

FIG. 13. Time series of background checks by state, from North Dakota to Wyoming.

REFERENCES

[1] Bureau of Alcohol Tobacco Firearms and Explosives, "Firearms commerce in the United States annual statistical update 2018," (2018), https://www.atf.gov/file/130436/download.

[2] Small Arms Survey, "Small Arms Survey 2007: Guns and the city," (2007), https://www.smallarmssurvey.org/resource/small-arms-survey-2007-guns-and-city.

[3] Bureau of Alcohol, Tobacco, Firearms and Explosives, "Questions and answers regarding the NICS system-ATF," Https://www.atf.gov/qa-category/national-instant-criminal-background-check-system-nics.

[4] L. R. Timsina, N. Qiao, A. C. Mongalo, A. N. Vetor, A. E. Carroll, and T. M. Bell, "National Instant Criminal Background Check and youth gun carrying," Pediatrics **145**, e20191071 (2020).

[5] M. Porfiri, R. R. Sattanapalle, S. Nakayama, J. Macinko, and R. Sipahi, "Media coverage and firearm acquisition in the aftermath of a mass shooting," Nature Human Behaviour **3**, 913–921 (2019).

[6] J. P. Schleimer, C. D. McCort, A. B. Shev, V. A. Pear, E. Tomsich, A. De Biasi, S. Buggs, H. S. Laqueur, and G. J. Wintemute, "Firearm purchasing and firearm violence during the coronavirus pandemic in the United States: a cross-sectional study," Injury Epidemiology **8**, 43 (2021).

[7] B. J. Lang and M. Lang, "Pandemics, protests, and firearms," American Journal of Health Economics **7**, 131–163 (2021).

[8] R. Ruddell and G. Mays, "State background checks and firearms homicides," Journal of Criminal Justice **33**, 127–136 (2005).

[9] B. Sen and A. Panjamapirom, "State background checks for gun purchase and firearm deaths: An exploratory study," Preventive Medicine **55**, 346–350 (2012).

[10] P. Levine and R. McKnight, "Firearms and accidental deaths: Evidence from the aftermath of the Sandy Hook school shooting," Science **358**, 1324–1328 (2017).

[11] M. Porfiri, R. Barak-Ventura, and M. Ruiz Marín, "Self-protection versus fear of stricter firearm regulations: Examining the drivers of firearm acquisitions in the aftermath of a mass shooting," Patterns **1**, 100082 (2020).

[12] E. Depetris-Chauvin, "Fear of Obama: An empirical study of the demand for guns and the U.S. 2008 presidential election," Journal of Public Economics **130**, 66–79 (2015).

[13] M. Luca, D. Malhotra, and C. Poliquin, "The impact of mass shootings on gun policy," Journal of Public Economics **181**, 104083 (2020).

[14] M. Eshbaugh-Soha and J. S. Peake, "Presidents and the economic agenda," Political Research Quarterly **58**, 121–138 (2005).

[15] Y. Kuramoto, *Chemical Oscillations, Waves, and Turbulence* (Springer, Berlin, Berlin, 1984).

[16] J. Peña Ramirez, L. Alberto Olvera, H. Nijmeijer, and J. Alvarez, "The sympathy of two pendulum clocks: beyond Huygens' observations," Scientific Reports **6** (2016).

[17] D. Harding and A. Pagan, "Synchronization of cycles," Journal of Econometrics **132**, 59–79 (2006).

[18] R. F. Galán, N. Fourcaud-Trocmé, G. B. Ermentrout, and N. N. Urban, "Correlation-induced synchronization of oscillations in olfactory bulb neurons," Journal of Neuroscience **26**, 3646–3655 (2006).

[19] G. Arnulfo, S. Wang, V. Myrov, B. Toselli, J. Hirvonen, M. Fato, L. Nobili, F. Cardinale, A. Rubino, A. Zhigalov, S. Palva, and J. M. Palva, "Long-range phase synchronization of high-frequency oscillations in human cortex," Nature Communications **11**, 5363 (2020).

[20] G. Dumas, "Towards a two-body neuroscience," Communicative & Integrative Biology **4**, 349–352 (2011).

[21] F. Alderisio, G. Fiore, and R. Salesse, "Interaction patterns and individual dynamics shape the way we move in synchrony." Scientific Reports **7**, 360–378 (2017).

[22] T. D. Frank and M. J. Richardson, "On a test statistic for the Kuramoto order parameter of synchronization: An illustration for group synchronization during rocking chairs," Physica D: Nonlinear Phenomena **239**, 2084–2092 (2010).

[23] M. Richardson, R. Garcia, T. Frank, M. Gergor, and K. Marsh, "Measuring group synchrony: A cluster-phase method for analyzing multivariate movement time-series," Frontiers in Physiology **3**, 405 (2012).

[24] M. G. Rosenblum, A. S. Pikovsky, and J. Kurths, "Phase synchronization of chaotic oscillators," Physical Review Letters **76**, 1804–1807 (1996).

[25] R. Quian Quiroga, T. Kreuz, and P. Grassberger, "Event synchronization: A simple and fast method to measure synchronicity and time delay patterns," Physical Review. E **66**, 041904 (2002).
[26] R. Quian Quiroga, J. Arnhold, and P. Grassberger, "Learning driver-response relationships from synchronization patterns," Physical Review. E **61**, 5142–5148 (2000).
[27] R. Quian Quiroga, A. Kraskov, T. Kreuz, and P. Grassberger, "Performance of different synchronization measures in real data: A case study on electroencephalographic signals," Physical Review. E **65**, 041903 (2002).
[28] J.-P. Lachaux, E. Rodriguez, J. Martinerie, and F. J. Varela, "Measuring phase synchrony in brain signals," Human Brain Mapping **8**, 194–208 (1999).
[29] S. H. Strogatz, "From Kuramoto to Crawford: exploring the onset of synchronization in populations of coupled oscillators," Physica D: Nonlinear Phenomena **143**, 1–20 (2000).
[30] J. Acebron, L. Bonilla, C. Vicente, F. Ritort, and R. Spigler, "The Kuramoto model: A simple paradigm for synchronization phenomena," Reviews of Modern Physics **77**, 137 (2005).
[31] B. Bag, K. Petrosyan, and C.-K. Hu, "Influence of noise on the synchronization of the stochastic Kuramoto model," Physical Review. E **76**, 056210 (2007).
[32] S. Marple, "Computing the discrete-time "analytic" signal via FFT," IEEE Transactions on Signal Processing **47**, 2600–2603 (1999).
[33] A. V. Oppenheim, *Discrete-Time Signal Processing* (Prentice-Hall, Inc, New Jersey, Upper Saddle River, NJ, 1998) pp. 366–369.
[34] H. Luo, X. Fang, and B. Ertas, "Hilbert transform and its engineering applications," AIAA Journal **47**, 923–932 (2009).
[35] J. Lilly and S. Olhede, "Higher-order properties of analytic wavelets," IEEE Transactions on Signal Processing **57**, 146–160 (2009).
[36] B. Kralemann, L. Cimponeriu, M. Rosenblum, A. Pikovsky, and R. Mrowka, "Phase dynamics of coupled oscillators reconstructed from data," Physical Review. E **77**, 066205 (2008).
[37] J. Gao, X. Dong, W.-B. Wang, Y. Li, and C. Pan, "Instantaneous parameters extraction via wavelet transform," IEEE Transactions on Geoscience and Remote Sensing **37**, 867–870 (1999).
[38] M. Le Van Quyen, J. Foucher, J.-P. Lachaux, E. Rodriguez, A. Lutz, J. Martinerie, and F. J. Varela, "Comparison of Hilbert transform and wavelet methods for the analysis of neuronal synchrony," Journal of Neuroscience Methods **111**, 83–98 (2001).
[39] P. Tass, M. G. Rosenblum, J. Weule, J. Kurths, A. Pikovsky, J. Volkmann, A. Schnitzler, and H.-J. Freund, "Detection of n:m phase locking from noisy data: Application to magnetoencephalography," Physical Review Letters **81**, 3291–3294 (1998).
[40] A. Potamianos and P. Maragos, "A comparison of the energy operator and the Hilbert transform approach to signal and speech demodulation," Signal Processing **37**, 95–120 (1994).
[41] M. Simon and G. R. Tomlinson, "Use of the Hilbert transform in modal analysis of linear and non-linear structures," Journal of Sound and Vibration **96**, 421–436 (1984).
[42] S. Kak, "The discrete Hilbert transform," Proceedings of the IEEE **58**, 585 – 586 (1970).
[43] D. Gupta and C. J. James, "Narrowband vs. broadband phase synchronization analysis applied to independent components of ictal and interictal EEG," 29th Annual International Conference of the IEEE Engineering in Medicine and Biology Society **2007**, 3864–3867 (2007).
[44] M. Meissner, "Accuracy issues of discrete Hilbert transform in identication of instantaneous parameters of vibration signals," Acta Physica Polonica A **121**, 164 (2012).
[45] E. Bedrosian, "A product theorem for Hilbert transforms," Proc. IEEE **51**, 868 (1963).
[46] R. R. Coifman and S. Lafon, "Diffusion maps," Applied and Computational Harmonic Analysis **21**, 5 – 30 (2006).
[47] A. Kolpas, J. Moehlis, T. A. Frewen, and I. G. Kevrekidis, "Coarse analysis of collective motion with different communication mechanisms," Mathematical Biosciences **214**, 49 – 57 (2008).
[48] M. Aureli, F. Fiorilli, and M. Porfiri, "Portraits of self-organization in fish schools interacting with robots," Physica D: Nonlinear Phenomena **241**, 908 – 920 (2012).
[49] R. Banisch and P. Koltai, "Understanding the geometry of transport: Diffusion maps for Lagrangian trajectory data unravel coherent sets," Chaos: An Interdisciplinary Journal of Nonlinear Science **27**, 035804 (2017).
[50] T. Sipola, A. Juvonen, and J. Lehtonen, "Anomaly detection from network logs using diffusion maps," (2011) pp. 172–181.
[51] S. Lafon and A. B. Lee, "Diffusion maps and coarse-graining: a unified framework for dimensionality reduction, graph partitioning, and data set parameterization," IEEE Transactions on Pattern Analysis and Machine Intelligence **28**, 1393–1403 (2006).
[52] B. Nadler, S. Lafon, R. R. Coifman, and I. G. Kevrekidis, "Diffusion maps-a probabilistic interpretation for spectral embedding and clustering algorithms," in *Principal manifolds for data visualization and dimension reduction* (Springer, Berlin, 2008) pp. 238–260.
[53] J. Shlens, "A tutorial on principal component analysis," arXiv preprint **arXiv:1404.1100** (2014).
[54] J. B. Tenenbaum, V. de Silva, and J. C. Langford, "A global geometric framework for nonlinear dimensionality reduction," (2000) pp. 2319–2323.
[55] Federal Bureau of Investigation, "National Instant Criminal Background Check System (NICS)-FBI," Https://www.fbi.gov/services/cjis/nics.
[56] R. E. Walpole, R. H. Myers, S. L. Myers, and K. E. Ye, *Probability and Statistics for Engineers and Scientists* (Pearson Education, Inc, Massachusetts, 2012) pp. 507–529.
[57] G. Strang and T. Nguyen, *Wavelets and Filter Banks* (Wellesley-Cambridge Press, Massachusetts, MA, 1996).
[58] W. H. Lee, E. Bullmore, and S. Frangou, "Quantitative evaluation of simulated functional brain networks in graph theoretical analysis," NeuroImage **146**, 724–733 (2017).
[59] G. Filatrella, N. Pedersen, and K. Wiesenfeld, "Generalized coupling in the Kuramoto model," Physical Review. E **75**, 017201 (2007).
[60] A. Nuttall, "Some windows with very good sidelobe behavior," IEEE Transactions on Acoustics, Speech, and Signal Processing **29**, 84–91 (1981).
[61] B. Nadler, S. Lafon, R. R. Coifman, and I. G. Kevrekidis, "Diffusion maps, spectral clustering and eigenfunctions of Fokker-Planck operators," arXiv preprint math/0506090 (2005).
[62] K. Parker, J. Horowitz, R. Igielnik, B. Oliphant, and A. Brown, "America's complex relationship with guns," (2017), pew Research Center.
[63] K. Rogers, "Black Friday gun sales soared, F.B.I. data shows," (2015), https://www.nytimes.com/2015/12/03/us/black-friday-gun-sales-soared-fbi-data-shows.html.
[64] L. Melgar, "The holiday season is big business for the gun industry," (2019), https://wamu.org/story/19/11/27/the-holiday-season-is-big-business-for-the-gun-industry/.
[65] L. Aguiar-Conraria, P. Brinca, H. V. Guðjónsson, and M. J. Soares, "Business cycle synchronization across US states," The BE Journal of Macroeconomics **17** (2017).
[66] X. Sheng, H. A. Marfatia, R. Gupta, and Q. Ji, "House price synchronization across the US states: The role of structural oil shocks," The North American Journal of Economics and Finance **56**, 101372 (2021).
[67] G. J. Wintemute, "The epidemiology of firearm violence in the twenty-first century United States," Annual Review of Public Health **36**, 5–19 (2015).
[68] D. Paradice, "An analysis of US school shooting data (1840-2015)." Education **138**, 135 – 144 (2017).
[69] L. A. Magee, "Community-level social processes and firearm shooting events: A multilevel analysis," Journal of Urban Health **97**, 296–305 (2020).
[70] S. Spitzer, D. Vail, L. Tennakoon, C. Rajasingh, D. Spain, and T. Weiser, "Readmission risk and costs of firearm injuries in the United States, 2010-2015," PLOS ONE **14**, e0209896 (2019).
[71] M. Livingston, M. Rossheim, and K. Hall, "A descriptive analysis of school and school shooter characteristics and the severity of school shootings in the United States, 1999–2018," Journal of Adolescent Health **64**, 797–799 (2019).
[72] J. Silver, A. Simons, and S. Craun, "A study of the pre-attack behaviors of active shooters in the United States between 2000 – 2013," (2018), federal Bureau of Investigation, U.S. Department of Justice.
[73] M. D. Makarios and T. C. Pratt, "The effectiveness of policies and programs that attempt to reduce firearm violence: A meta-analysis," Crime & Delinquency **58**, 222–244 (2012).
[74] A. Croitoru, S. Kien, R. Mahabir, J. Radzikowski, A. Crooks, R. Schuchard, T. Begay, A. Lee, A. Bettios, and A. Stefanidis, "Responses to mass shooting events," Criminology & Public Policy **19**, 335–360 (2020).

[75]J. M. Pierre, "The psychology of guns: risk, fear, and motivated reasoning," Palgrave Communications **5**, 159 (2019).
[76]M. Docherty, E. Mulvey, J. Beardslee, G. Sweeten, and D. Pardini, "Drug dealing and gun carrying go hand in hand: Examining how juvenile offenders' gun carrying changes before and after drug dealing spells across 84 months," Journal of Quantitative Criminology **36**, 993–1015 (2020).
[77]E. L. Sevigny and A. Allen, "Gun carrying among drug market participants: Evidence from incarcerated drug offenders," Journal of Quantitative Criminology **31**, 435–458 (2015).
[78]C. Loeffler and S. Flaxman, "Is gun violence contagious? A spatiotemporal test," Journal of Quantitative Criminology **34**, 999–1017 (2018).
[79]A. Braga, A. Papachristos, and D. Hureau, "The concentration and stability of gun violence at micro places in Boston, 1980–2008," Journal of Quantitative Criminology **26**, 33–53 (2010).
[80]J. Xu and E. Griffiths, "Shooting on the street: Measuring the spatial influence of physical features on gun violence in a bounded street network," Journal of Quantitative Criminology **33(2)**, 237–253 (2017).